Multifractal detrended fluctuation analysis: Practical applications to financial time series

James R. Thompson,[a] James R. Wilson[b,*]

[a]*MITRE Corporation, 7515 Colshire Dr., McLean, VA 22102, USA*

[b]*Edward P. Fitts Department of Industrial and Systems Engineering, North Carolina State University, Campus Box 7906, Raleigh, North Carolina 27695-7906, USA*

Abstract

To analyze financial time series exhibiting volatility clustering or other highly irregular behavior, we exploit multifractal detrended fluctuation analysis (MF-DFA). We summarize the use of local Hölder exponents, generalized Hurst exponents, and the multifractal spectrum in characterizing the way that the sample paths of a multifractal stochastic process exhibit light- or heavy-tailed fluctuations as well as short- or long-range dependence on different time scales. We detail the development of a robust, computationally efficient software tool for estimating the multifractal spectrum from a time series using MF-DFA, with special emphasis on selecting the algorithm's parameters. The software is tested on simulated sample paths of Brownian motion, fractional Brownian motion, and the binomial multiplicative process to verify the accuracy of the resulting multifractal spectrum estimates. We also perform an in-depth analysis of General Electric's stock price using conventional time series models, and we contrast the results with those obtained using MF-DFA.

Key Words and Phrases: financial time series, generalized Hurst exponent, long-range dependence, monofractal process, multifractal detrended fluctuation analysis, multifractal process, multifractal spectrum, self-similar process, short-range dependence.

[a]Corresponding author. Edward P. Fitts Department of Industrial and Systems Engineering, North Carolina State University, Campus Box 7906, Raleigh, North Carolina 27695-7906, USA. Telephone: (919) 515-6415. Fax: (919) 515-5281.

E-mail address: jwilson@ncsu.edu.

1. Introduction

The analysis of economic systems relies heavily on time series data. Many types of financial time series, most notably market returns, have been found to exhibit long-range memory as well as dramatic day-to-day fluctuations that cannot be adequately represented by light-tailed distributions such as the normal distribution. In particular, this means that for such time series, the usual variance parameter (i.e., the sum of covariances at all time lags) is not defined because the covariance function does not converge to zero sufficiently fast as the time lag increases. Moreover in such time series, often the tails of the marginal density converge to zero so slowly that higher-order marginal moments such as skewness and kurtosis fail to exist. Conventional autoregressive–moving average (ARMA) models [4] for analyzing time series data cannot accommodate these properties; and various extensions of ARMA models such as generalized autoregressive conditional heteroscedastic (GARCH) models also fall short of capturing the true erratic nature of empirical data [3].

As early as 1900, researchers began modeling financial time series using highly irregular stochastic processes such as Brownian motion. A Brownian motion process $\{X(t) : t \geq 0\}$ is self-similar with sample paths that are continuous, nondifferentiable, and have Hölder exponent $\alpha = 0.5$ at every time $t \geq 0$. Roughly speaking, the latter property means that for each $t \geq 0$, the increment $X(t+s) - X(t)$ of the process is with high probability of the order of $|s|^{0.5}$ as the time-interval length $|s| \to 0$; and this result is easily verified because $X(t+s) - X(t)$ is normally distributed with mean zero and standard deviation equal to $|s|^{0.5}$ for all $t \geq 0$ and $|s| \leq t$. Mandelbrot's pioneering work in geometry later showed that the sample paths of such highly irregular processes have a Hausdorff dimension strictly exceeding their topological dimension [17]. He used the term *fractal* to refer to geometric objects with this property, and he went on to generalize the concept to more complex geometric objects known as *multifractals*.

In many application domains, a real-valued multifractal stochastic process $\{X(t) : t \in [0,T]\}$ with $0 < T < \infty$ has self-similar behavior; furthermore over each time interval $[t, t+s]$, the magnitude of the associated increment $X(t+s) - X(t)$ is with high probability of the order of $|s|^{\alpha(t)}$ as $|s| \to 0$, where the local Hölder exponent $\alpha(t)$ is nonnegative and may vary as a function of the interval's initial (or reference) time t. If q is in $\mathscr{Q}$, a certain neighborhood of zero that contains the unit interval $[0,1]$, then the generalized Hurst exponent $h(q)$ is defined in terms of the qth absolute moment of $X(t)$ for each $t \in [0,T]$; and in contrast to the local Hölder exponents, $h(q)$ is a global characteristic of the process over the entire time horizon $[0,T]$. Derived from the generalized Hurst exponents $\{h(q) : q \in \mathscr{Q}\}$, the multifractal spectrum $f(\alpha)$ for $\alpha \geq 0$ provides a concise description of the following: (i) the general arrangement of the local Hölder exponents over the time horizon of the process; and (ii) the way the sample paths of the process exhibit light- or

heavy-tailed fluctuations as well as short- or long-range dependence on different time scales. To estimate the multifractal spectrum of a stochastic process from a time series realization of that process, Kantelhardt et al. [12] formulate an approach known as multifractal detrended fluctuation analysis (MF-DFA).

Applications of fractal and multifractal analyses have increased dramatically in recent years. Bao et al. [1] study the dissolution of particles in a solvent by using fractal analysis to characterize the changes in particle-surface geometry during dissolution and the associated changes in the chemical reactivity of particle surfaces. Lopes et al. [15] demonstrate the effectiveness of multifractal analysis for representing volumetric texture in 3D medical imaging. Tharmin, Stern, and Frey [24] provide evidence that both morphology and physiological signals of the body exhibit fractal properties, and they argue that these properties may predict future risk of disease.

Beyond engineering and the physical and medical sciences, researchers in the social sciences are discovering fractals in the signals from complex adaptive systems such as financial markets; and this in turn has led economists to apply fractal analysis to long-debated theories like the efficient market hypothesis [8]. To characterize the efficiency of European equity markets, Onali and Goddard [21] apply monofractal analysis to the following European stock market indices: ASE (Amsterdam), CDAX (Frankfurt), FTSE 350 (London), Mibtel (Milan), MSE (Madrid), and SWX (Zurich). For comparison, the authors also apply monofractal analysis to PX-Glob, the index for the emerging stock market of Prague, as well as the DJIA (New York). The authors reach the following conclusions:

- There is highly significant evidence that the emerging stock market index PX-Glob exhibits long-range dependence.
- There is marginally significant evidence of long-range dependence in the smaller stock market indices MSE and SWX.
- There is no evidence of long-range dependence for the other five stock market indices (ASE, CDAX, FTSE 350, Mibtel, and DJIA).

However, Onali and Goddard note that allowing the Hurst exponents to differ between higher and lower frequencies reveals a departure from simple random walk behavior. This begs the question of whether fluctuations of some sizes might exhibit more persistent (i.e., long-range dependent) behavior, while fluctuations of other sizes might exhibit antipersistent (i.e., short-range dependent) behavior. Unfortunately monofractal analysis based on the rescaled range cannot represent such complex phenomena, whereas multifractal analysis is specifically designed to answer these questions.

Mulligan and Koppl [20] use fractal analysis to quantify the changes in macromonetary stability during the period that Alan Greenspan served as chair of the Federal Reserve's Board of Governors. The macroeconomic time series of primary interest are monthly observations of monetary aggregates, ratios, and multipliers for the years 1987–2006. Mulligan and Koppl employ only monofractal analysis, but they use five different techniques to estimate the Hurst exponent for each time series. They state that conventional statistical models and econometric techniques are unable to distinguish completely random components from deterministic ones in a complex system, and as such fractal techniques must be employed. The authors' results indicate an increase in antipersistent behavior, suggesting that decision-makers consistently overreact to new information and never learn not to overreact. Although this information is gained a posteriori, it provides a valuable insight for the policymakers at the Federal Reserve about how their strategies are perceived by the market. Unfortunately the authors had to employ multiple methods for estimating the relevant fractal properties; and none of these methods are capable of detecting the complex multifractal properties often present in financial data.

Tivnan et al. [28] combine simulations of financial markets with multifractal analysis as a method for validating their simulation results against real financial data. The authors start by first recreating the so-called "stylized facts" of financial time series in their simulation as detected by conventional econometrics. They then go a step further and compare the S&P 500 with their simulation results using multifractal analysis. The added benefit of multifractal analysis is that multifractals provide a perspective on structure rather than value, and thus give insight into the mechanisms that create the stylized facts evident in the time series.

In this article, we detail a robust, computationally efficient software implementation of MF-DFA to analyze financial time series. In Section 2 we discuss the use of local Hölder exponents, generalized Hurst exponents, and the multifractal spectrum in characterizing a multifractal stochastic process. In Section 3 we detail our implementation of MF-DFA as a method for estimating the multifractal spectrum from a given time series, with special emphasis on selecting the algorithm's parameters in large-scale practical applications. In Section 4 we discuss the results of applying the MF-DFA software to simulated sample paths of selected processes whose multifractal spectra are known—namely, Brownian motion, fractional Brownian motion, and the binomial multiplicative process. In Section 5 we summarize the results of analyzing the time series of General Electric (GE) stock prices during the period 2000–2003 using conventional time series analysis (namely, ARMA, GARCH, and ARMA+GARCH models); and we exploit the results of multifractal time series analysis of the GE data to explain the lack of fit observed with conventional time series models. Thompson and Wilson [25] present a preliminary, abridged version of some of the material detailed in Sections 2 and 5 of this article. A related paper [26] details the application of MF-DFA to price

paths generated by agent-based simulations of financial markets.

2. Multifractal detrended fluctuation analysis (MF-DFA)

In this article we restrict attention to self-similar stochastic processes, as exemplified by Brownian motion because an increment of Brownian motion over a fixed time interval $[t, t+s]$ is a suitably rescaled probabilistic replica of Brownian motion over the much smaller time interval $[t, t+\eta s]$ when $0 < \eta \ll 1$; and when $\eta \gg 1$, a similar relationship holds. The stochastic process $\{X(t) : t \in \mathbb{R}\}$ is said to be self-similar with Hurst exponent $H \geq 0$ if for any $\eta > 0$ we have

$$\{X(t) : t \in \mathbb{R}\} \stackrel{\mathrm{d}}{=} \left\{ \eta^{-H} X(\eta t) : t \in \mathbb{R} \right\}, \tag{1}$$

where $\stackrel{\mathrm{d}}{=}$ denotes equality in distribution. It follows from Equation (1) that the increments of a self-similar process satisfy the relation $X(t+s) - X(t) \stackrel{\mathrm{d}}{=} \eta^{-H}[X(t+\eta s) - X(t)]$ for all $t, s \in \mathbb{R}$ and $\eta > 0$. Examination of self-similar data sets in the context of time series analysis shows that the Hurst exponent characterizes the asymptotic behavior of the autocorrelation function (ACF) of the time series [2]. Values of H in the interval $(0.5, 1.0)$ lead to positive autocorrelations that decay too slowly for the sum of autocorrelations over all lags to be finite. Processes with $0.5 < H < 1$ are said to exhibit long-range dependence (long memory); and processes with $0 \leq H \leq 0.5$ are said to exhibit short-range dependence (short memory).

A process with $0 < H < 0.5$ exhibits *antipersistence* in its sample paths, which means that a positive increment (increase) in the process is more likely to be followed by a negative increment (decrease) in the next nonoverlapping time interval and vice versa; and this tendency of the process to turn back on itself results in sample paths with a very rough structure. When $0.5 < H < 1$, the process exhibits *persistence*, which means that successive nonoverlapping increments in the process are more likely to have the same sign; and smoother sample paths result from this tendency of the process to persist in its current direction of movement. Therefore in a self-similar process with Hurst exponent H (that is, a "monofractal" process), H quantifies not only the asymptotic behavior of the ACF but also the inherent roughness of the sample paths of the process. The Hausdorff dimension D of the sample path of a monofractal Gaussian process (i.e., fractional Brownian motion) is related to the Hurst exponent of the underlying process by the relation $H = 2 - D$; see Theorem 16.7 of Falconer [7]. For example, Brownian motion has $H = \alpha = 0.5$; and every sample path of Brownian motion has Hausdorff dimension $D = 1.5$.

For a self-similar stochastic process $\{X(t) : t \in [0, T]\}$, we define the Hölder exponent $\alpha(t)$ at each time $t \in [0, T]$ as follows:

$$\alpha(t) = \sup\left\{ \beta \geq 0 : X(t+s) - X(t) = O_P\big[|s|^{\beta}\big] \text{ as } |s| \to 0 \right\},$$

where in general for continuous-time stochastic processes $\{A(s) : s \in \mathbb{R}\}$ and $\{B(s) : s \in \mathbb{R}\}$, the "big Oh in probability" notation $A(s) = O_P[B(s)]$ as $|s| \to 0$ means that given an arbitrarily small $\zeta > 0$, there is a constant $M = M(\zeta)$ and a positive number $\varepsilon = \varepsilon(\zeta)$ such that $\Pr\{\, |A(s)| \le M|B(s)| \,\} \ge 1 - \zeta$ for $|s| < \varepsilon$. Roughly speaking, the relationship $X(t+s) - X(t) = O_P\big[|s|^{\,\alpha(t)}\big]$ at time t as $|s| \to 0$ means that the process increment $X(t+s) - X(t)$ is with high probability of the order of $|s|^{\,\alpha(t)}$ as the time-interval length $|s|$ tends to zero while the initial time t remains fixed; moreover, the Hölder exponent $\alpha(t)$ is defined for every t in the given time horizon $[0,T]$.

One way to think of a multifractal process $\{X(t) : t \in [0,T]\}$ is as the amalgamation of an infinite number of monofractal subprocesses, each characterized by a single Hölder exponent α. However, these monofractal processes are interwoven throughout the time horizon $[0,T]$ such that the set of time points associated with any one monofractal process constitutes a fractal set.

DEFINITION 1. *A self-similar stochastic process* $\{X(t) : t \in [0,T]\}$ *is* multifractal *if it satisfies*

$$\mathrm{E}\big[\, |X(t)|^q \,\big] = c(q)t^{\tau(q)+1} \text{ for all } t \in \mathscr{G} \text{ and } q \in \mathscr{Q},$$

where: $0 < T < \infty$ *;* $\mathscr{G}$ *and* $\mathscr{Q}$ *are open intervals on* $\mathbb{R}$*;* $[0,T] \subset \mathscr{G}$*; and* $[0,1] \subset \mathscr{Q}$.

The function $\tau(q)$ is called the *scaling function* of the multifractal process [5]. The scaling function is concave [5, Proposition 1]; and except in trivial cases, its second derivative $\mathrm{d}^2\tau(q)/\mathrm{d}q^2$ is negative for all $q \in \mathscr{Q}$ [7, p. 287]. Kantelhardt et al. [12, Section 2.2] explain the basis for the relationship

$$\tau(q) = qh(q) - 1 \quad \text{for all} \quad q \in \mathscr{Q} \tag{2}$$

between the scaling function $\tau(q)$ and the generalized Hurst exponent $h(q)$. It follows from (2) that $\mathrm{d}\tau(q)/\mathrm{d}q = h(q) + q\big[\mathrm{d}h(q)/\mathrm{d}q\big]$ for all $q \in \mathscr{Q}$.

If for a fixed $q \in \mathscr{Q}$ we define the set of points

$$\mathscr{T}_q = \left\{ t \in [0,T] : \alpha(t) = h(q) + q\frac{\mathrm{d}h(q)}{\mathrm{d}q} \right\} \tag{3}$$

and if we let $\alpha = \alpha_q$ denote the common value of the Hölder exponent $\alpha(t)$ for all $t \in \mathscr{T}_q$, then the multifractal spectrum $f(\alpha)$ evaluated at $\alpha = \alpha_q$ is defined to be the Hausdorff dimension of the set $\mathscr{T}_q$ [7, Section 2.2]. The multifractal spectrum $f(\alpha)$ can also be computed from the relation

$$f(\alpha) = \min_{q \in \mathscr{Q}} \{\, q\alpha - \tau(q) \,\} \quad \text{for} \quad \alpha \ge 0, \tag{4}$$

which is the Legendre transform of $\tau(q)$ for $q \in \mathscr{Q}$ [5, Theorem 6]. The function $f(\alpha)$ describes key properties of a multifractal time series as follows:

- The Hölder exponents $\{\alpha(t) : t \in [0,T]\}$ specify how the underlying stochastic process $\{X(t) : t \in [0,T]\}$ fluctuates as we examine its increments computed from nonoverlapping time intervals whose common length is systematically varied over a broad range of values.

- For a particular nonnegative value α_0 of the Hölder exponent, the corresponding value $f(\alpha_0)$ of the multifractal spectrum is the Hausdorff dimension of the subset of time points $t \in [0,T]$ at which the stochastic process $\{X(t) : t \in [0,T]\}$ has its Hölder exponent $\alpha(t) = \alpha_0$.

Although $f(\alpha)$ is not a proper probability density function for $\alpha \geq 0$, in its "renormalized" form as specified by Equation (4), for each fixed α_0 the associated function value $f(\alpha_0)$ represents in some sense the general arrangement of the set of time points at which the multifractal process $\{X(t) : t \in [0,T]\}$ has the specific value α_0 for its Hölder exponent [5, Section IV.A].

The multifractal spectrum $f(\alpha)$ is defined for $\alpha \in [\alpha_{\min}, \alpha_{\max}] \subset [0, \infty)$, achieving the value of 1 at its unique global maximum; and if $\alpha_{\min} < \alpha_{\max}$, then $f(\alpha)$ is concave with negative second derivative for $\alpha \in (\alpha_{\min}, \alpha_{\max})$ [7, pp. 286–289]. If a stochastic process is monofractal, then it has a single Hölder exponent that coincides with its Hurst exponent H and describes how its increments behave locally at all time points; and therefore the multifractal spectrum of a monofractal process with Hurst exponent H is given by

$$f(\alpha) = \begin{cases} 1, & \text{if } \alpha = H, \\ 0, & \text{if } \alpha \neq H \text{ and } \alpha \geq 0, \end{cases} \tag{5}$$

so that $\alpha_{\min} = \alpha_{\max} = H$. These various interpretations are collectively referred to as the multifractal formalism, and they provide the basis for our intuition about the multifractal spectrum. They also lead to methods for estimating the multifractal spectrum from a given time series.

3. Implementation of the MF-DFA algorithm

Among the most effective methods for estimating the multifractal spectrum $f(\alpha)$ from a time series, multifractal detrended fluctuation analysis (MF-DFA) is the easiest to implement and the most robust [12]. In Section 3.1 we present a formal algorithmic statement of MF-DFA as we have implemented it in Java for large-scale practical applications. In Section 3.2 we discuss how to select key parameters of MF-DFA, including: (i) a preprocessing algorithm to determine the degree m of the polynomial that in Step 3 of MF-DFA must be fitted to the data within each segment of the time series; (ii) the finite set $\mathscr{S}$ of values for the segment length s to be used in Steps 2 through 5 of MF-DFA; and (iii) the finite set $\mathscr{Q}'$ of values for the moment order q to be used in Steps 4 through 6 of MF-DFA.

3.1. Algorithmic statement of MF-DFA

The MF-DFA algorithm, as presented by Kantelhardt et al. [12], has five steps, the first three of which are the same as for detrended fluctuation analysis (DFA) [22]. However, a critical distinction regarding the format of the data may eliminate the first step (see Section 3.2). In our formulation of MF-DFA, we also incorporate the final step of calculating $f(\alpha)$ from the scaling function $\tau(q)$, for a total of six steps.

MF-DFA Algorithm

Step 1: Ensure that the data set $\{Y(n) : n = 1,\ldots,N\}$ of length N is an "aggregated" data set as opposed to a "disaggregated" data set. An example of a disaggregated data set would be daily price increments (i.e., returns) of an asset, while an aggregated data set would be the actual daily price (i.e., the accumulated daily price increments). If starting from an original time series $\{U_k : k = 1,\ldots,N+1\}$ of length $N+1$ we have at some point switched to working with the disaggregated data set $\{x_k = U_{k+1} - U_k : k = 1,\ldots,N\}$ of first differences of the original data set or if only the disaggregated data set $\{x_k\}$ is available, then we must convert $\{x_k\}$ to an aggregated data set by computing the cumulative sums

$$Y(n) = \sum_{k=1}^{n} \left(x_k - \bar{x}\right) \quad \text{for} \quad n = 1,\ldots,N,$$

where $\bar{x} = (1/N)\sum_{k=1}^{N} x_k$ denotes the sample mean of the disaggregated observations.

Step 2: Let $\mathscr{S}$ denote a predetermined set of positive integer values for the segment length s that satisfy $20 \le s \le N/10$. For each $s \in \mathscr{S}$, divide the aggregated data set $\{Y(n) : n = 1,\ldots,N\}$ into $N_s = \lfloor N/s \rfloor$ nonoverlapping segments of length s. If N is not a multiple of s, then repeat the procedure starting at the other end of the data set. Throughout the remaining discussion of MF-DFA, we assume that N is not a multiple of s; and in this situation creating $2N_s$ segments ensures every data point is used in the analysis.

Step 3: For $\nu = 1,\ldots,N_s$, the νth nonoverlapping segment of the aggregated observations consists of the subseries $\{Y[(\nu-1)s+i] : i = 1,\ldots,s\}$; similarly for $\nu = N_s+1,\ldots,2N_s$, the νth segment consists of the subseries $\{Y[N-(\nu-N_s)s+i] : i = 1,\ldots,s\}$. For the νth segment ($\nu = 1,\ldots,2N_s$) and a value of m determined in a preprocessing algorithm (see Section 3.2.2), fit a degree-m polynomial $y_\nu(i)$ to the aggregated observations in that segment. Calculate the maximum likelihood estimator of the corresponding residual variance in segment ν,

$$F^2(\nu,s) = \frac{1}{s}\sum_{i=1}^{s} \left\{ Y[(\nu-1)s+i] - y_\nu(i) \right\}^2 \quad \text{for} \quad \nu = 1,\ldots,N_s,$$

and

$$F^2(\nu,s) = \frac{1}{s}\sum_{i=1}^{s}\left\{ Y[N-(\nu-N_s)s+i] - y_\nu(i)\right\}^2 \quad \text{for} \quad \nu = N_s+1,\ldots,2N_s.$$

Step 4: Let $\mathscr{Q}'$ denote a predetermined finite subset of $\mathscr{Q}$ that contains zero as well as positive and negative values of the moment order q. For a given segment length $s \in \mathscr{S}$ and for each $q \in \mathscr{Q}'$, calculate the order-q fluctuation function from the residual variance estimates $\left\{ F^2(\nu,s) : \nu = 1,\ldots,2N_s \right\}$ as follows:

$$F_q(s) = \left\{ \frac{1}{2N_s}\sum_{\nu=1}^{2N_s}\left[F^2(\nu,s)\right]^{q/2} \right\}^{1/q} \quad \text{for} \quad q \in \mathscr{Q}'\setminus\{0\},$$

and

$$F_0(s) = \exp\left\{ \frac{1}{4N_s}\sum_{\nu=1}^{2N_s}\ln\left[F^2(\nu,s)\right] \right\}.$$

Repeat steps 2 to 4 for each segment length $s \in \mathscr{S}$.

Step 5: For each $q \in \mathscr{Q}'$, perform a linear regression of the response variable $\ln\left[F_q(s)\right]$ on the predictor variable $\ln(s)$ for all $s \in \mathscr{S}$; and using the slope of the fitted linear function as an estimator of $h(q)$, compute an estimator of $\tau(q)$ from the relationship 2 for each $q \in \mathscr{Q}'$.

Step 6: From the estimator of the function $\tau(q)$ and for each $q_0 \in \mathscr{Q}'$, estimate the derivative

$$\alpha_0 = \left.\frac{d\tau(q)}{dq}\right|_{q=q_0} \quad \text{for each} \quad q \in \mathscr{Q}'; \tag{6}$$

and finally estimate the multifractal spectrum from the relation

$$f(\alpha_0) = q_0\alpha_0 - \tau(q_0) \quad \text{for} \quad q_0 \in \mathscr{Q}'.$$

3.2. Selecting parameters of the MF-DFA algorithm

3.2.1. Form of the data: aggregated or disaggregated

When Peng et al. [22] first proposed DFA, they did so in the context of analyzing DNA nucleotide sequences. To convert a DNA sequence into a time series suitable for statistical analysis, they first assigned the value -1 to each purine in the sequence, and they assigned the value $+1$ to each pyrimidine in the sequence. They then defined the "DNA walk" as the displacement of the walker after n steps. If x_n denotes the value assigned to the nth nucleotide in a given DNA sequence for $n = 1,2,\ldots$, then the displacement of the walker on the nth step of the DNA walk is given by the cumulative sum $Y(n) = \sum_{k=1}^{n} x_k$ for $n = 1,2,\ldots$. The disaggregated data set $\{x_n : n = 1,2,\ldots\}$ represents the one-step increments of the aggregated data set $\{Y(n) : n = 1,2,\ldots\}$

that we seek to analyze. Kantelhardt et al. [12] recommend converting a disaggregated data set into the corresponding aggregated data set as the first step of the MF-DFA algorithm. However, if the data is already aggregated (such as the daily closing price of an asset), then this step should be eliminated.

3.2.2. Determining the range of scales and the polynomial fit

Before invoking the MF-DFA algorithm, in a preprocessing algorithm we determine the following: (i) the degree m of the polynomial that in Step 3 of MF-DFA must be fitted to the data within each segment of length s; and (ii) the finite set $\mathscr{S}$ of values of the segment length s to be used in Steps 2 through 5 of MF-DFA. Kantelhardt et al. [12] note that for small values of the segment length (i.e., $s \leq 10$), the polynomial regression in Step 3 of MF-DFA will be performed on too few data points; and thus the residual variance estimators $F^2(\nu,s)$ will not be sufficiently stable. Similarly, for $s \geq N/4$, there will be too few segments yielding the estimators $F^2(\nu,s)$ from which we compute the order-q fluctuation function $F_q(s)$; and thus the latter statistic will not be sufficiently stable. These general guidelines indicate that we must have $10 \leq s \leq N/4$. However, such a range could potentially be very broad for a financial time series.

In practice we have found that substantial experimentation can be required to determine appropriate settings for the minimum value $s_{\min}$ and the maximum value $s_{\max}$ of the time scale (segment length) s to be used in Steps 2 through 5 of MF-DFA. Although a true multifractal process in continuous time exhibits self-similar behavior on a continuum of time scales ranging from arbitrarily small to arbitrarily large values of s, a finite-length time series realization of such a process can only reveal multifractal behavior on a finite set $\mathscr{S}$ of values for s. Any implementation of MF-DFA should thus allow the user to manipulate $s_{\min}$ and $s_{\max}$ as well as the increment size Δ_s used to iterate from $s_{\min}$ to $s_{\max}$. We present the following guidelines as a good starting point, but we recommend carefully considering the time interval represented by the data before applying these guidelines:

$$s_{\min} = \max\{20, N/100\}, \quad s_{\max} = \min\{20 s_{\min}, N/10\}, \quad \text{and} \tag{7}$$

$$\Delta_s = \frac{s_{\max} - s_{\min}}{100}. \tag{8}$$

The guidelines (7) and (8) ensure that enough data points are available for the polynomial regressions performed in Step 3 of MF-DFA and that a sufficient number of residual variance estimators $F^2(\nu,s)$ are available for estimating the order-q fluctuation function $F_q(s)$. The increment Δ_s is designed to provide exactly 100 points for the doubly-logarithmic linear regression in Step 5 of MF-DFA. Note that for high-frequency financial data with over half a million data points in a one-year time span, we found that $s_{\min} =$ 1 day and $s_{\max} = 20$ days (i.e., one month of trading days) typically worked well. The minimum $s_{\min}$ also

suggests an upper bound of 18 for the degree m of the polynomials fitted in Step 3 of MF-DFA (note that $s \geq m+2$ is required in order to perform the regression). In practice, this bound is not likely to be needed (see below), but it gives a convenient terminating condition for the software implementation.

The overall concept of MF-DFA is to estimate the generalized Hurst exponent $h(q)$ for each selected moment order $q \in \mathscr{Q}'$, where $h(q)$ is the slope of the theoretical linear regression of $\ln\left[F_q(s)\right]$ on $\ln(s)$ for $s \in \mathscr{S}$. However, strong trends in the (aggregated) time series can bias the regression-based estimator of $h(q)$; and thus in Step 3 of MF-DFA, it is critical to determine an adequate degree m of the polynomial fitted to the subseries of observations within each segment of length s. If the fitted polynomial $y_\nu(i)$ of degree m in each segment ν does not adequately represent the trend in that segment, then the plot of $\ln\left[F_q(s)\right]$ versus $\ln(s)$ for $s \in \mathscr{S}$ in Step 5 of MF-DFA will display a noticeable departure from linearity in the form of a sharp upward bend (or "dogleg") that suggests a crossover from one generalized Hurst exponent to another in the time series [11, <Section 3.2]. Recall that the generalized Hurst exponent is a global property and thus should not change for a given value of q. Such a crossover would cause the estimated linear regression of $\ln\left[F_q(s)\right]$ on $\ln(s)$ in Step 5 of MF-DFA to yield a poor fit and thus a biased estimator of $h(q)$. This problem is eliminated, however, if the degree m equals or exceeds the degree of the inherent trend in the observations within each segment, which suggests a convenient algorithm for avoiding this pitfall.

Although there are many statistical methods that we could perform to estimate the degree m of the polynomial to be fitted to the observations within each segment of length s in Step 3 of MF-DFA, we found that the heuristic procedure outlined below is easy to implement and yields reliable results rapidly and automatically. This procedure was adapted from Kuhl, Sumant, and Wilson [13], who implemented it in the context of multiresolution analysis for modeling and simulation of nonstationary arrival processes exhibiting nested periodic effects as well as a long-term trend in the underlying arrival rate. Note that the preprocessing algorithm given below uses only the moment order $q = 2$.

Preprocessing Algorithm for MF-DFA

Step P0: Initialize the tolerance level $\delta \leftarrow 0.01$ for testing the adequacy of the polynomial fit of degree $m \leftarrow 1$ to the observations within each segment, and the significance level $\omega \leftarrow 0.05$ to be used in the likelihood ratio test for evaluating the adequacy of a degree-m polynomial fit as m is iteratively increased. Based on Equations (7) and (8), initialize $J \leftarrow 101$ and the set of segment lengths $\mathscr{S} \leftarrow \left\{ s_j = s_{\min} + (j-1)(s_{\max} - s_{\min})/(J-1) : j = 1, \ldots, J \right\}$. Fix the moment order $q \leftarrow 2$.

Step P1: Perform Steps 2 thru 5 of the MF-DFA algorithm.

Step P2: From the linear regression equation fitted to the logged data

$$\left\{ \left(\ln(s_j), \ln\left[F_q(s_j)\right] \right) : j = 1, \ldots, J \right\} \tag{9}$$

in Step 5 of MF-DFA, compute the associated error sum of squares (SSE_m) and the total sum of squares (SST_m); and compute the ratios

$$G \leftarrow \frac{\mathrm{SSE}_m}{\mathrm{SST}_m} \quad \text{and} \quad \mathrm{MSE}_m = \frac{\mathrm{SSE}_m}{J}.$$

Step P3: If $G \leq \delta$, then a linear regression provides an adequate fit to the logged data in Step 5 of MF-DFA; deliver the current value of m and stop. If $G > \delta$, then set $m \leftarrow m+1$ and go to Step P4.

Step P4: Reperform Steps 2 through 5 of MF-DFA using the current value of m, yielding the updated logged data set (9); and recompute MSE_m from the linear regression performed on that data set.

Step P5: Compute the likelihood ratio test statistic

$$\chi^2_{\mathrm{test}} = -J \ln\left(\frac{\mathrm{MSE}_m}{\mathrm{MSE}_{m-1}} \right). \tag{10}$$

If the polynomial of degree $m-1$ yields an adequate fit to the original (aggregated) observations within each segment so that a linear regression yields an adequate fit to the updated logged data set (9), then the test statistic (10) has approximately a chi-squared distribution with 1 degree of freedom. Therefore, (10) is used to test the null hypothesis that a polynomial of degree $m-1$ provides an adequate fit to the original observations within each segment versus the alternative hypothesis that the degree of the polynomial is at least m within each segment.

Step P6: If $\chi^2_{\mathrm{test}} \leq \chi^2_{1-\omega,1}$ then deliver m and stop. If $\chi^2_{\mathrm{test}} > \chi^2_{1-\omega,1}$, then set $m \leftarrow m+1$ and return to Step P4.

It should be noted that when implementing these procedures, there is always the potential for errors being introduced through the finite precision inherent in modern computers. Specifically, if the values of the order-q fluctuation function $F_q(s)$ are close to zero, then their logged values will approach negative infinity. These results can introduce error into the calculation of the multifractal spectrum. Overfitting the polynomial regression should thus be avoided. This is handled first by ensuring a large enough value of $s_{\min}$ and second by minimizing m as much as possible. Based on our computational experience, we concluded that the above procedures generally avoided this pitfall when the data set was large enough and was inherently multifractal. On the other hand, we obtained unreliable results with these procedures when they were applied to complex data sets that did not exhibit multifractal behavior.

3.3. Numerical approximations

The last issue we address with MF-DFA is the obvious error introduced by taking numerical approximations to derivatives in the calculation of each α. In the implementation of MF-DFA, the most convenient approach to estimating the Hölder exponent as in Equation (6) is to iterate over a range of q-values centered at zero for uniform increments Δq. Then the value of the desired Hölder exponent is approximated by

$$\alpha_0 \approx \frac{\tau(q_0+\Delta q)-\tau(q_0)}{\Delta q} \text{ for each } q_0 \in \mathscr{Q}'. \tag{11}$$

It has been noted that for large values of $|q|$, the error in the multifractal spectrum tails becomes large [14]. In our implementation we choose $\Delta q = 0.1$; and we iterate between $q_{\min} = -5$ and $q_{\max} = 5$, which is within the suggested range for q and yields

$$\mathscr{Q}' = \{-5 + j(0.1) : j = 0, 1, \ldots, 100\}.$$

Choosing $\Delta q = 0.1$ allows for a sufficient number of $h(q)$ values to minimize the discretization error in Equation (11). However, care should be taken for the particular data set in question. Ideally, the range for q and the value for Δq should be parameters that the user can manipulate easily when running MF-DFA.

4. Applying MF-DFA software to known multifractals

Our software implementation of MF-DFA incorporates functions for generating known fractal and multifractal time series. However, recall that fractals possess infinite detail such that examining finer and finer scales only reveals more and more detail or roughness. Clearly a computer simulation of a finite number of points imposes a limit on the amount of detail that can be captured experimentally. We found that simulated monofractals produced sharply peaked multifractal spectra with the following properties: (i) the values of $f(\alpha)$ were all between roughly 0.8 and 1.0; and (ii) the associated values of α were clustered around the estimated expected value of α, which was usually very close to the dominant Hölder exponent predicted by theory. Recall also that multifractal analysis generally concerns the identification of short- or long-range dependence in a time series as characterized by the generalized Hurst exponents $\{h(q) : q \in \mathscr{Q}\}$ or the corresponding multifractal spectrum $f(\alpha)$ as defined for the Hölder exponents $\{\alpha\}$ specified in Equation (3).

Although the identification of short- or long-range dependence in a time series is often straightforward, precisely estimating the degree of self-similarity is notoriously difficult. By applying Hurst's rescaled range approach to subsets of the time series of yearly minimum water levels of the Nile river, Beran [2, p. 84] obtains estimates of H that clearly exceed 0.5 but exhibit substantial variation, with the smallest and largest

estimates of H being 0.856 and 1.17, respectively. This makes statistical inference about the true value of H difficult at best.

The net result for the practitioner is that MF-DFA can effectively discriminate between the following situations:

- multifractal self-similarity that results from a broad range of Hölder exponents (characterized by q-dependence in the generalized Hurst exponents); or
- monofractal self-similarity that results from a narrow range of Hölder exponents (characterized by little or no q-dependence in the generalized Hurst exponents).

MF-DFA can also indicate the relative size of the generalized Hurst exponents (or the associated Hölder exponents) in the data and thus can detect short- and long-range dependence. However, when the Hölder exponents $\{\alpha\}$ defining the estimated multifractal spectrum $f(\alpha)$ are tightly clustered in the neighborhood of 0.5, it is not generally possible to make definitive statements about the presence of short- or long-range dependence. Mandelbrot [18, Section 7.3] shows the nonuniversality of the multifractal spectrum, so the primary value of multifractal analysis on finite-length time series must be based on the comparison of one multifractal spectrum with another. If the spectra produced by two different time series exhibit the same properties, then we can infer that the probabilistic mechanisms driving the two underlying processes are similar.

4.1. Application to Brownian motion and fractional Brownian motion

Because nonoverlapping increments of standard Brownian motion for fixed-length time intervals are independent identically distributed (i.i.d.) normal random variables with mean zero and variance equal to the fixed time-interval length, it is relatively straightforward to generate an adequate approximation to sample paths of standard Brownian motion. For this process, we do not expect the generalized Hurst exponent $h(q)$ to exhibit dependence on the moment order q; and therefore MF-DFA is expected to yield an estimate of the multifractal spectrum that is tightly concentrated near the point $(\alpha, f(\alpha)) = (0.5, 1.0)$. Figure 1(a) shows $N = 2^{16}$ data points of simulated standard Brownian motion, and Figure 1(b) shows the multifractal spectrum obtained via MF-DFA. The interpretation of this multifractal spectrum is that the time series exhibits Hölder exponents in the neighborhood of 0.5. In this case the estimated mean value of α is approximately 0.48.

For $0 < H < 1$, fractional Brownian motion $\{B_H(t) : t \geq 0\}$ is a Gaussian process with stationary incre-

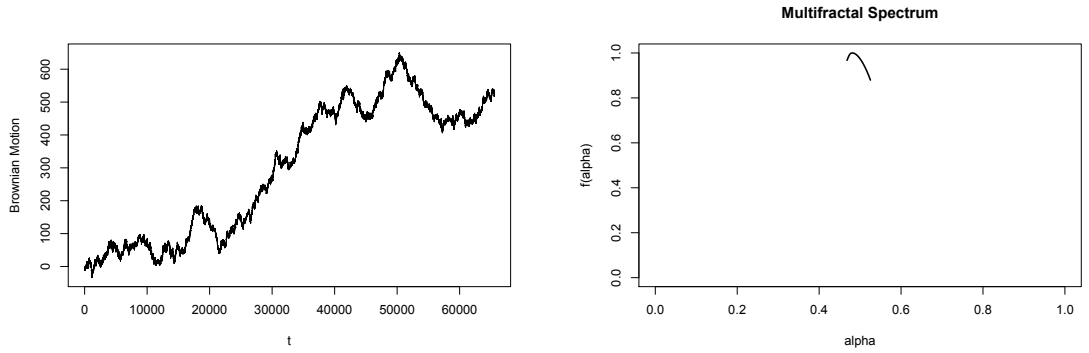

(a) An approximation of standard Brownian motion (b) Multifractal spectrum of simulated Brownian motion

Fig. 1. Testing MF-DFA on Brownian motion.

ments, mean zero, variance $\mathrm{E}\left[B_H^2(t)\right] = t^{2H}$, and covariance function

$$\mathrm{Cov}\left[B_H(t_1), B_H(t_2)\right] = 0.5\left[t_1^{2H} + t_2^{2H} - \left|t_1 - t_2\right|^{2H}\right] \quad \text{for} \quad t_1, t_2 \geq 0\,.$$

It can be shown that the disaggregated process $\{X_i : i = 1, 2, \ldots\}$ defined by the increments of fractional Brownian motion,

$$X_i = B_H(i) - B_H(i-1) \;\text{ for }\; i = 1, 2, \ldots\,, \tag{12}$$

has the covariance function

$$\gamma(\ell) = \mathrm{Cov}(X_i, X_{i+\ell}) = 0.5\left[(\ell+1)^{2H} - 2\ell^{2H} + |\ell-1|^{2H}\right] \text{ for } \ell = 0, 1, \ldots\,;$$

see Taqqu and Teverovsky [23]. Particularly noteworthy is the asymptotic behavior of $\gamma(\ell)$ as the lag ℓ approaches infinity. If $H \neq 0.5$, then we have

$$\gamma(\ell) \sim 2H(2H-1)\ell^{2H-2} \text{ as } \ell \to \infty\ . \tag{13}$$

If $0.5 < H < 1$, then Equation (13) implies that $\sum_{\ell=0}^{\infty} |\gamma(\ell)| = \infty$ so the process (12) exhibits long-range dependence. On the other hand if $0 < H \leq 0.5$, then $0 < \sum_{\ell=0}^{\infty} |\gamma(\ell)| < \infty$ so the process (12) exhibits short-range dependence. If $H = 0.5$, then $\{B_H(t) : t \geq 0\}$ is standard Brownian motion; and the increments $\{X_i : i = 1, 2, \ldots\}$ are i.i.d. standard normal.

Using the fArma package in R, we generated time series realizations of length $N = 2^{16}$ for fractional Brownian motion with $H = 0.6$ and $H = 0.8$ [31]. The two plots of fractional Brownian motion are shown in Figure 2(a), separated arbitrarily for visual clarity. The parameter H in fractional Brownian motion is the same at all scales, meaning that such a process is monofractal. Therefore we expect a time series realization of fractional Brownian motion to exhibit a multifractal spectrum that is concentrated near the single point

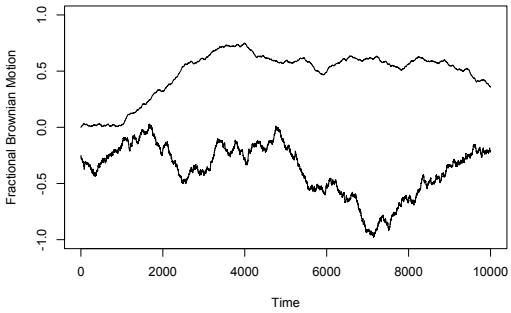

(a) Fractional Brownian motion: $H = 0.8$ (top) and $H = 0.6$ (bottom)

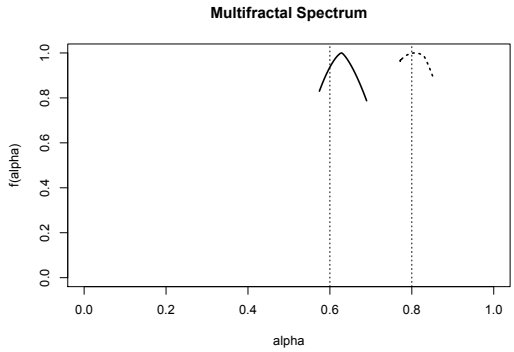

(b) Multifractal spectra: $H = 0.6$ (solid) and $H = 0.8$ (dotted)

Fig. 2. Testing MF-DFA on fractional Brownian motion.

$(\alpha, f(\alpha)) = (H, 1)$. This property is confirmed in Figure 2(b), which displays the estimated multifractal spectra for $H = 0.6$ and $H = 0.8$.

Kantelhardt et al. [12, Section 4] explain why randomly shuffling the dependent increments of fractional Brownian motion with $H \neq 0.5$ is expected to yield a pronounced change in the associated multifractal spectrum; on the other hand, randomly shuffling the independent increments of standard Brownian motion is not expected to yield any change in the associated multifractal spectrum. Figure 3 shows the results applying MF-DFA to the shuffled increments of standard Brownian motion compared with the spectrum of the original series. Although there is some change in the multifractal spectrum of the shuffled increments of standard Brownian motion, it is still clustered around the theoretical value $\alpha = 0.5$.

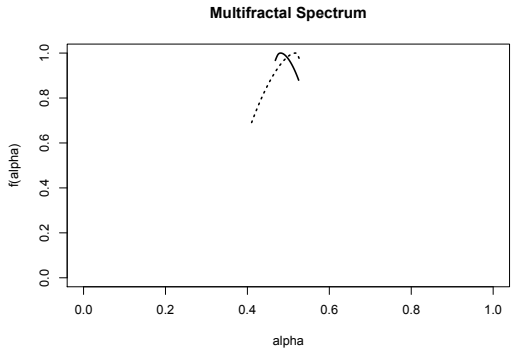

Fig. 3. Multifractal spectra of standard Brownian motion: original series (solid), shuffled series (dotted).

Similarly, Figures 4(a) and 4(b) show the same comparison for the fractional Brownian motion processes with $H = 0.6$ and $H = 0.8$, respectively. In these cases, the shuffled multifractal spectra in Figures 4(a) and 4(b) respectively exhibit substantial shifts away from the neighborhoods of $\alpha = 0.6$ and $\alpha = 0.8$. We concluded from Figures 4(a) and 4(b) that in each case, the original increments of fractional Brownian

motion exhibited definitive evidence of long-range dependence.

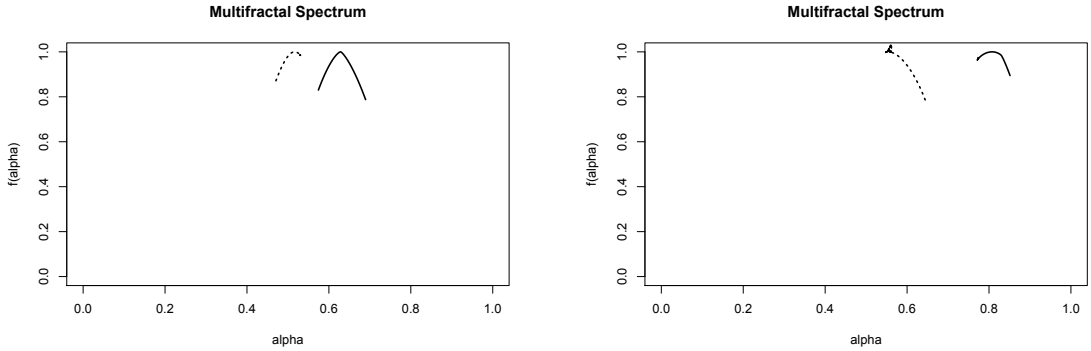

(a) Shuffle test for fractional Brownian motion ($H = 0.6$) (b) Shuffle test for fractional Brownian motion ($H = 0.8$)

Fig. 4. Shuffle test: original series is solid, shuffled series is dotted.

4.2. Application to binomial multiplicative process

A standard example of a multifractal process is the binomial multiplicative process [9, Section 6.2], which is also called the binomial measure [5]. The binomial measure on the unit interval $[0,1]$ is constructed by a simple iterative procedure. Let w_0 and w_1 denote positive masses or weights such that $w_0 + w_1 = 1$ and $w_0 \neq 0.5$. On the first iteration of the procedure, the unit interval is divided in half, with the mass w_0 being spread uniformly over the left-hand half and the complementary mass w_1 being spread uniformly over the right-hand half. At the beginning of the ℓth iteration ($\ell = 2, \ldots$), the unit interval consists of $2^{\ell-1}$ nonoverlapping segments, each of length $1/2^{\ell-1}$ and each with its own uniform distribution of mass that was assigned on the previous iteration so that the total mass summed over all segments is one. Then on the ℓth iteration, each segment is divided in half, with the fraction w_0 of the segment's mass being spread uniformly over the left-hand half and the complementary fraction w_1 of the segment's mass being spread uniformly over the right-hand half. It can be shown that in the limit as the number of iterations tends to infinity, this procedure ultimately yields a probability measure on the unit interval whose cumulative distribution function (c.d.f.) is continuous and nondifferentiable (i.e., singular) [5]. Figures 5(a) and 5(b) illustrate this property for 2^{16} points generated with $w_0 = 0.25$.

Close examination of Figures 5(a) and 5(b) reveals a self-similar structure as we would expect with any fractal. However, the binomial measure is a multifractal and therefore should exhibit a broader multifractal spectrum than the multifractal spectra for the fractional Brownian motion processes discussed in the previous section. Because of the simplicity of the method for constructing the binomial measure, we can derive a closed-form expression for its associated multifractal spectrum. Specifically the generalized Hurst exponent

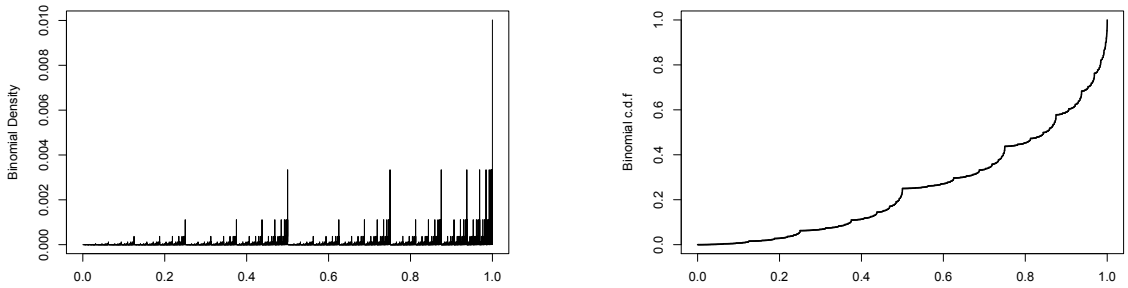

(a) The density of 2^{16} points of the multifractal binomial measure

(b) The cumulative multifractal binomial measure

Fig. 5. The multifractal binomial measure with $w_0 = 0.25$.

of order $q \in \mathscr{Q} = \mathbb{R}$ is given by

$$h(q) = \begin{cases} q^{-1} - \ln\left(w_0^q + w_1^q\right)/[q\ln(2)], & \text{if } q \neq 0, \\ -\ln(w_0 w_1)/[2\ln(2)], & \text{if } q = 0. \end{cases} \tag{14}$$

Then the multifractal spectrum is given parametrically as follows:

$$\alpha = h(q) + q\frac{\mathrm{d}h(q)}{\mathrm{d}q} \quad \text{and} \quad f(\alpha) = q[\alpha - h(q)] + 1 \quad \text{for} \quad q \in \mathscr{Q}; \tag{15}$$

see, for example, Kantelhardt et al. [12, Equations (16) and (20)]. It follows from Equations (14) and (15) that α can take any value between $-\ln(w_0)/\ln(2)$ and $-\ln(w_1)/\ln(2)$. The expected value of α is given by $-\ln(w_0 w_1)/[2\ln(2)]$, which corresponds to the unique maximum value of one for the multifractal spectrum. Figure 6 shows the results of applying MF-DFA to the time series plotted in Figure 5(b). For $w_0 = 0.25$, the Hölder exponents ranges from 0.415 to 2.00 with expected value 1.21. This is in close agreement with the estimate of the multifractal spectrum delivered by MF-DFA.

Next we investigate the source of the multifractal properties in the binomial measure using the shuffling heuristic. Note in Figure 5(a) how the increments tend to cluster together in a predictable pattern. The pattern gets ever larger as we move from left to right; but the smallest increments are always on the left, followed by increments of progressively increasing sizes as we move to the right. Shuffling the increments will break up this pattern of dependence and therefore substantially alter the associated multifractal spectrum. Figure 6 illustrates the impact of shuffling a multifractal time series that exhibits long-range dependence. There is a notable change in the multifractal spectrum, as it shrinks to a set of Hölder exponents clustered around 0.5.

In the preceding example, we constructed a deterministic multifractal process such that on each iteration we always applied the weight w_0 to the left-hand half of each segment and the weight w_1 to the right-hand half of that segment. On the other hand, if for each segment at each iteration we randomly select the weight

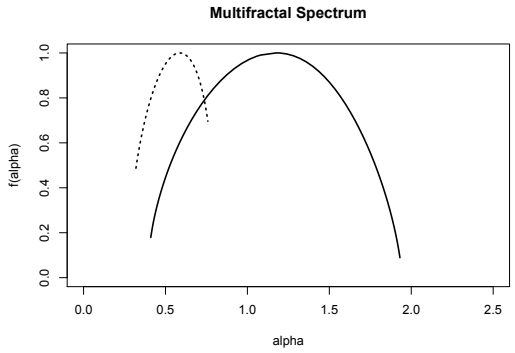

Fig. 6. The multifractal spectrum of the multifractal binomial measure (solid) and the resulting spectrum from the shuffled series (dotted).

(w_0 or w_1) to apply to the left-hand half of the segment and the complementary weight is applied to the right-hand half of that segment, then we obtain a stochastic version of the binomial measure. Stochastic versions of a similar multinomial measure are used to model trading time in the multifractal model of asset returns developed by Calvet and Fisher [5]. Such processes no longer possess the well-organized self-similarity seen in Figure 5(a), but rather they exhibit a statistical self-similarity. For example, compare Figure 5(a) with the plotted increments of the stochastic binomial measure shown in Figure 7(a). Although the two plots differ considerably in appearance, they were constructed with the same weights $w_0 = 0.25$ and $w_1 = 0.75$; and the deterministic binomial measure can be regarded as merely one specific realization of the stochastic binomial measure. Now for each realization of the stochastic binomial measure, MF-DFA delivers an estimate of the theoretical multifractal spectrum for the limiting stochastic process characterized by the fixed weights w_0 and w_1. Consequently for the deterministic and stochastic binomial measures with the same weights w_0 and w_1, applying MF-DFA to a time series of length N from each process should yield an estimated multifractal spectrum that will converge to the same theoretical multifractal spectrum as $N \to \infty$. Figure 7(b) displays the results of applying MF-DFA to time series of length $N = 2^{16}$ from both the deterministic and stochastic binomial measures; and clearly the two estimated multifractal spectra nearly coincide.

The above examples illustrate the value of multifractal analysis. The sample path of Brownian motion shown in Figure 1 appears to be considerably more erratic than that of the binomial measure in Figure 5(b). But the underlying process of Brownian motion scales as a single Hurst exponent H (or Hölder exponent α) at every point, while the binomial measure displays a spectrum of Hölder exponents across sets of points that are interwoven throughout the unit interval and possess Hausdorff (fractal) dimensions between zero and one. Thus the relative complexity of the two processes was not immediately evident through comparison of their sample paths, but plotting their multifractal spectra together (see Figure 8) revealed the difference more

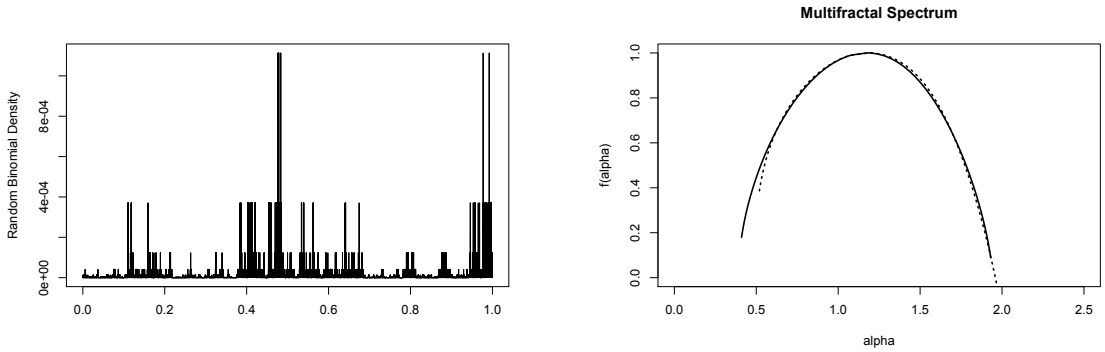

(a) The density of a stochastic multifractal binomial measure (b) Deterministic (solid) and stochastic (dotted)

Fig. 7. The stochastic multifractal binomial measure with $w_0 = 0.25$.

clearly. Moreover, the increments of the deterministic binomial measure shown in Figure 5(a) appeared to be quite different in structure from the increments of the stochastic binomial measure shown in Figure 7(a), yet multifractal analysis strongly indicated that the two processes were generated by fundamentally the same probabilistic mechanism.

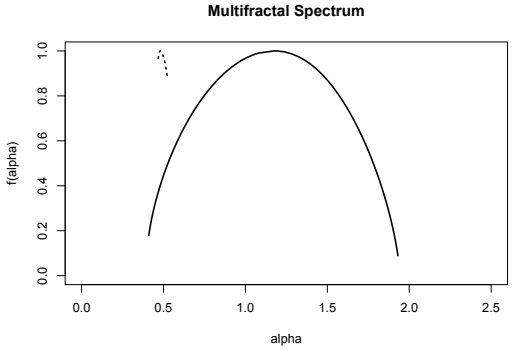

Fig. 8. The multifractal spectra of the binomial measure (solid) and standard Brownian motion (dotted)

We concluded that our implementation of MF-DFA functioned as intended and allowed us to gain some insight into the probabilistic mechanisms underlying a particular time series as compared with other stochastic processes. If a series exhibits long-range dependence, then we can employ the shuffling heuristic paired with MF-DFA to detect this type of time dependence. And when two time series appear to behave similarly, we can illuminate their true similarities (or fundamental differences) by plotting their multifractal spectra together.

5. Analysis of General Electric's stock price

In this section we apply MF-DFA to a high-frequency data set from the New York Stock Exchange. North Carolina State University's Department of Economics has access to stock exchange data on very fine scales as provided by Wharton Research Data Services (WRDS) [29]. WRDS was established in 1993 to assist research faculty at the University of Pennsylvania. Part of the function of WRDS has been to compile trade and quote (TAQ) data from various exchanges into a database to facilitate fine-scale analysis. In the sections that follow, we conduct an in-depth analysis of the multifractal properties of the TAQ price of the stock of General Electric (GE) as extracted from the WRDS database for the period 2000–2003.

The adjusted daily closing price of GE stock going back to 1962 is freely available from various online sources (see Figure 9(a)). To put the TAQ data set in perspective, the daily closing price from 1962 to 2012 consists of 12,786 data points, while the TAQ data from 2000 to 2003 (delimited by the vertical dashed lines in Figure 9(a)) consists of 4,273,056 data points. The TAQ data for the period 2000 to 2003 is shown in Figure 9(b).

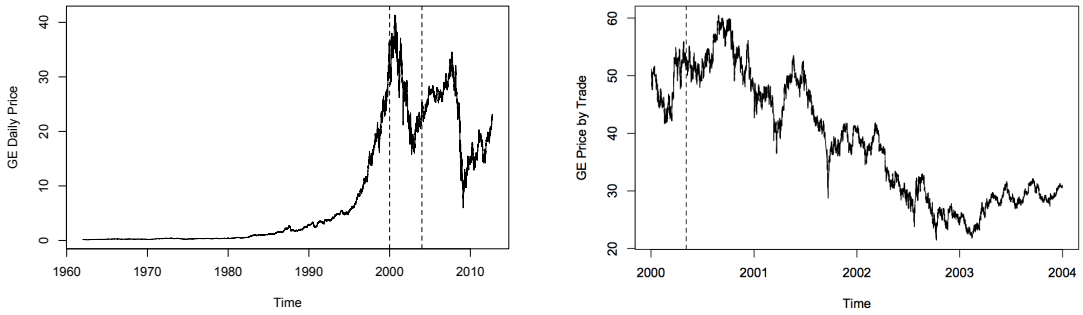

(a) GE's adjusted daily closing price: 1962 to 2012 **(b)** GE's TAQ price: 2000 to 2003

Fig. 9. GE stock-price time series.

On May 8, 2000, GE issued a three-to-one split of its shares; and the price dropped from \$156.38 to \$52.13 from the market closing on Friday, May 5, 2000, to the first trade on Monday, May 8, 2000. To adjust the price for this split, we divided by 3 each TAQ price up to May 5, 2000. The date of the split is shown by the vertical dashed line in Figure 9(b). Any other adjustments that may have been incorporated in the data set shown in Figure 9(a) are not incorporated in the TAQ data. For the years 2000, 2002, and 2003, there were 252 trading days throughout the year. In 2001, the terrorist attacks on September 11^{th} resulted in four less trading days for that year so that 2001 consisted of 248 trading days. Trading volume increased steadily during the period from 2000 to 2003. For the 252 trading days of 2000, there were on average 3,233 trades per day. By 2003 this number had increased to roughly 5,327 trades per day. See Table 1 for a

complete description of the TAQ time series for GE stock.

Table 1 GE TAQ data for calendar years 2000–2003

Year	Trades	Trading Days	Average Trades per Day	Splits
2000	814,728	252	3,233	May 8th – 3:1
2001	808,669	248	3,261	None
2002	1,307,249	252	5,188	None
2003	1,342,410	252	5,327	None

5.1. Traditional time series analysis

The first step in our analysis was a simple visual inspection of the time series $\{Y(n) : n = 1,\ldots,N\}$ of GE TAQ prices and the associated series $\{x_n = Y(n+1) - Y(n) : n = 1,\ldots,N-1\}$ of first differences. Figure 9(b) presented in the previous section shows the typical rough nature of financial data and what appears to be a strong downward trend from a high of \$60.50 until it levels out around \$30.00. There are also a couple of large changes in price that stand out, indicating the possibility of heavy tails in the underlying stochastic process. The plot of the first differences $\{x_n\}$, Figure 10(a), gives a clearer picture of the size of the changes in the price and the volatility within the series. By visual inspection alone, we concluded that the volatility was not constant. However, the first difference did appear to have stabilized the mean, bringing the data closer to a stationary series.

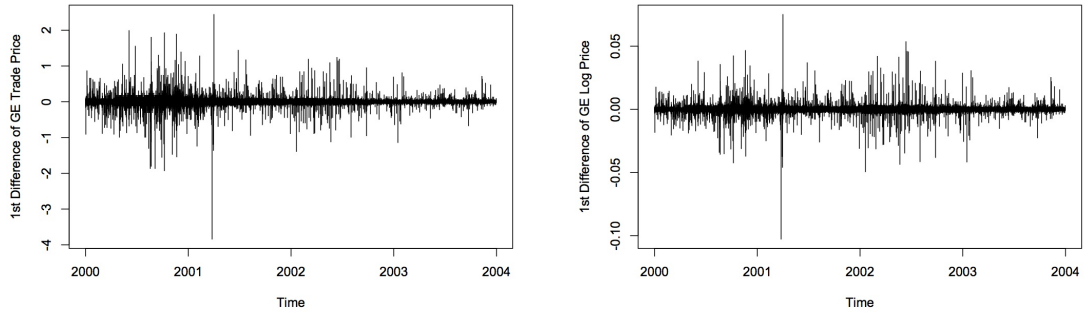

(a) The first difference of the GE TAQ data **(b)** The first difference of the log-price GE TAQ data

Fig. 10. GE stock price increments.

When working with financial data, it is customary to analyze the log-returns—i.e., the time series

$$\left\{z_n = \ln[Y(n+1)/Y(n)] : n = 1,\ldots,N-1\right\}. \tag{16}$$

Using this approach, we can convert multiple assets to the same scale. The hope is that the disaggregated, log-transformed series $\{z_n\}$ will represent a stationary stochastic process with a more tractable dependency

structure. We applied this transformation to the GE TAQ data; but based on Figure 10(b), we concluded that the log-returns also exhibited nonconstant variance and large jumps.

The results of this simple visual analysis suggested that the GE TAQ price data might exhibit the following properties: (i) a time dependence in the mean that could be removed by differencing; and (ii) a nonconstant variance that cannot removed by working with log-returns defined by Equation (16).

A reasonable choice for a model of the original time series $\{Y(n)\}$ of GE TAQ prices might therefore be a GARCH model or an ARMA+GARCH model. Note that a GARCH model assumes a constant mean, but a nonconstant variance. An ARMA+GARCH model allows for both the mean and the variance to depend on past realizations of the time series. For illustrative purposes we also analyzed the autocorrelation function (ACF) and partial autocorrelation function (PACF) of the original data. A widely used method for determining the parameters of an ARMA(p, q) model is to analyze these two functions together [4]. A sharp drop-off in the ACF at lag ℓ suggests a moving average model of order $q = \ell$, while a sharp drop-off at lag ℓ in the PACF suggests an autoregressive model of order $p = \ell$. Figure 11 shows the ACF trailing off well beyond a lag of 60, while the PACF drops off around lag $\ell = 4$.

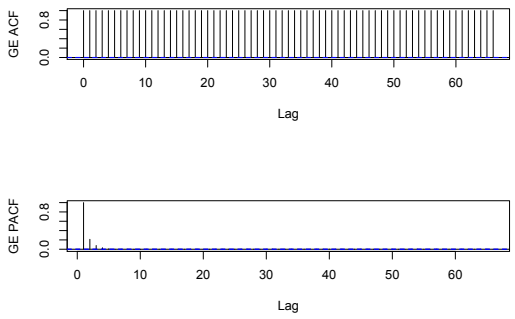

Fig. 11. The autocorrelation function (top) and partial autocorrelation function (bottom) of the GE TAQ data.

Visual inspection of the ACF suggested that the series might be nonstationary, because the ACF did not appear to exhibit any decline out to lag $\ell = 70$. However, the visual inspection of the PACF supported the conclusion that much of the autocorrelation at longer lags was simply due to the autocorrelation at the shorter lags being carried over through the time series. The PACF filters out this "carry-over" correlation and thus reveals the fundamental dependency structure of the process. Therefore we concluded that an AR(p) model would be appropriate for this particular time series, where $p \leq 4$.

When fitting an ARMA(p, q) model to a time series, it is good practice to minimize the values of p and q so as to avoid overparameterization and the associated problems of numerical and statistical instability. To identify an appropriate order p for an AR(p) model of the time series of GE TAQ prices, we sought to

minimize the Akaike Information Criterion (AIC) by incrementing the value of p systematically. Table 2 summarizes the results of this analysis. The AIC analysis showed a drastic improvement in the model fit in going from $p = 0$ to $p = 1$; but additional improvements in the model fit dropped off rapidly for $p \geq 2$, which suggested that the autoregressive order $p = 4$ was certainly large enough and might even be too large.

Table 2 GE TAQ Data: Akaike Information Criterion for AR(p), $p = 0, 1, \ldots, 4$

Parameter p	AIC(p)	$100[\Delta\text{AIC}(p)]\%$
0	31,842,229	
1	−20,953,846	−165.81%
2	−21,209,901	−1.22%
3	−21,252,219	−0.20%
4	−21,260,093	−0.037%

The results of the above exploratory analysis illustrate the challenge of time series analysis, particularly in the field of finance. Our initial visual inspection suggested a nonconstant variance may be governing the underlying process and thus pointed to a GARCH model. But the heuristic for identifying an appropriate ARMA model—coupled with a quick analysis of the changes in AIC—suggested that an AR(4) would be an appropriate description of the price path. In actuality, neither model proved to be a good fit for the GE TAQ data. The results of the AR(4) model suggested GE's TAQ price from 2000 to 2003 was described by

$$Y(n) = \mu_Y + \left\{ \sum_{\ell=1}^{4} \varphi_\ell \left[Y(n-\ell) - \mu_Y \right] \right\} + \varepsilon(n), \tag{17}$$

where $\varphi_1 = 0.731$, $\varphi_2 = 0.159$, $\varphi_3 = 0.068$, and $\varphi_4 = 0.043$, and $\mu_Y = 36.07$ is the steady-state mean TAQ price. However, the Box-Ljung-Pierce portmanteau lack-of-fit test on the estimated residuals $\{\widehat{\varepsilon}(n)\}$ out to lag $\ell = 20$ yielded a p-value of less than 2.2×10^{-16} and therefore led us to conclude that the estimated residuals were highly correlated and that Equation (17) was an inadequate model of the GE TAQ data. To further illustrate the inadequacy of the time series model (17), we constructed a Q-Q plot of the estimated residuals. Based on visual inspection of Figure 12, we concluded that the tails of the distribution of estimated residuals were much heavier than the tails of a normal distribution. These conclusions were confirmed by the chi-squared goodness-of-fit test that resulted in a p-value less than 2.2×10^{-16}.

The lack of fit exhibited by the AR(4) model is perhaps not surprising since we noted in our visual inspection that the data exhibited a nonconstant variance, suggesting that a GARCH model or an AR+GARCH model might be more appropriate. But fitting a GARCH(1,1) model to the GE TAQ data produced similarly inadequate results [27].

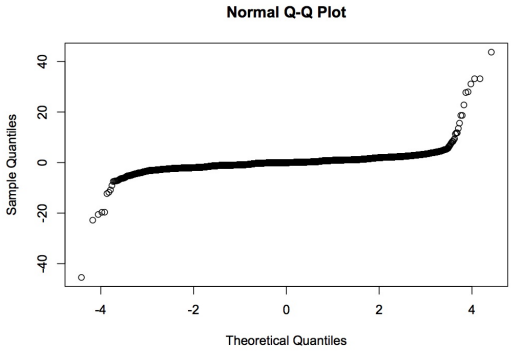

Fig. 12. A Q-Q plot of the residuals of the AR(4) model fit to the GE TAQ data.

Given the failure of the AR(4) and the GARCH(1,1) models separately, we took the exploratory analysis a step further and attempted to fit the log-returns with an AR(4)+GARCH(1,1) model defined as

$$z_n = \mu_z + \left\{ \sum_{\ell=1}^{4} \varphi_\ell \left[z_{n-\ell} - \mu_z \right] \right\} + \sigma_n u_n,$$

where

$$\sigma_n^2 = \vartheta_0 + \vartheta_1 \left(z_{n-1} - \mu_z \right)^2 + \psi_1 \sigma_{n-1}^2 \,,$$

and the $\{u_n\}$ are i.i.d. standard normal random variables. Unfortunately, given the size of the data set (and perhaps its complexity), the fGARCH package in R [30] encountered a singularity error and was unable to fit the combined AR(4)+GARCH(1,1) model to the time series (16) of log-returns. We systematically reduced the number of parameters in the combined model in an attempt to avoid the singularity error; and we even scrubbed the data to remove transactions that were made at the same price (i.e., zero returns). Nevertheless, we were unable to obtain a combined AR(4)+GARCH(1,1) model for log-returns; and thus we attempted to fit an AR(4)+GARCH(1,1) model to the log-prices

$$\{ Z(n) = \ln[Y(n)] : n = 1, \ldots N \} \,, \tag{18}$$

which is of course the aggregated process corresponding to the disaggregated log-return process (16).

We encountered a similar difficulty in fitting an AR(4)+GARCH(1,1) model to the log-prices (18); but ultimately we were successful in fitting an AR(2)+GARCH(1,1) model to the log-prices. Unfortunately the AR(2)+GARCH(1,1) model also failed the standard lack-of-fit tests. The Q-Q plot of the residuals from the AR(2)+GARCH(1,1) model of the logged GE TAQ prices (18) is shown in Figure 13, and the histogram of the residuals is shown in Figure 14. The skewness and excess kurtosis of the residuals of the combined model were -0.34 and -1.17 respectively. Based on all this evidence, we concluded that the AR(2)+GARCH(1,1) model failed to provide an adequate representation of the logged GE TAQ prices (18).

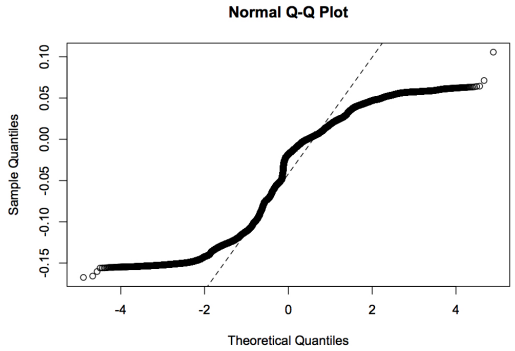

Fig. 13. The Q-Q plot of the residuals of the AR(2)+GARCH(1,1) model fit to the log GE TAQ data.

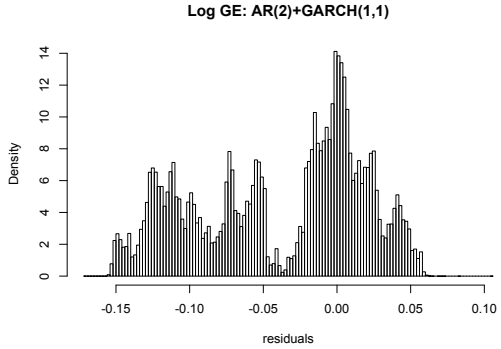

Fig. 14. The histogram of the residuals of the AR(2)+GARCH(1,1) model fit to the log GE TAQ data.

5.2. Multifractal time series analysis

In addition to the traditional tests and models, we investigated the scaling properties of the GE data using MF-DFA. One advantage of multifractal analysis is that there is no reason to transform the time series with logarithms or other operations. The intent of multifractal analysis is to analyze the changes in fluctuations over different time scales, and thus the raw (i.e., undifferenced and unlogged) trades or the adjusted daily closing prices are all that is required [10]. The multifractal spectrum exhibited by the GE TAQ data is shown in Figure 15. Recall that the GE TAQ data consists of over 4 million data points, and the number of daily trades ranged from 3,000 to roughly 5,000. When performing MF-DFA we set $s_{\min} = 3,000$ and $s_{\max} = 400,000$, with increments of $\Delta s = 7{,}000$. This amounts to analyzing fluctuations in an interval of about one day all the way up to an interval of about six months in roughly two-day increments. We also allowed the moment order q to range from -5 to 5. The spectrum peaks around $\alpha = 0.51$, indicating the dominant fluctuations in the process were similar to standard Brownian motion might exhibit short-range dependence, but there was a wide spectrum ranging from $\alpha = 0.30$ to $\alpha = 0.70$. This indicated that

large fluctuations, accentuated by positive q-values, tended to be antipersistent, while small fluctuations, accentuated by negative q-values, tend to be persistent and show long memory.

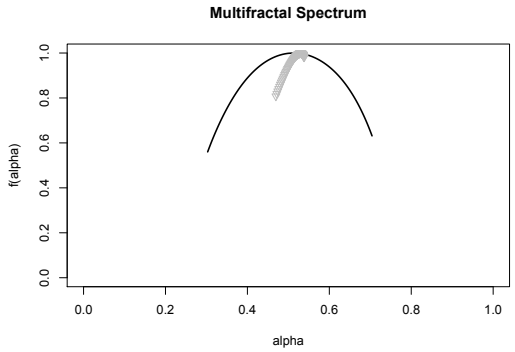

Fig. 15. The multifractal spectrum of the GE TAQ data (solid/black) and a shuffled version of the series (triangles/gray).

Employing the heuristic of shuffling the increments of a time series and analyzing the multifractal properties of the shuffled series reinforces our assertion that the small fluctuations exhibit long memory. The multifractal spectrum of the shuffled series is shown in comparison with the original GE TAQ multifractal spectrum in Figure 15. There is a notable change in the spectrum, as the shuffled series appears to be more monofractal, with most of its Hölder exponents clustered around $\alpha = 0.5$.

Finally, we simulated time series from the AR(4) model, the GARCH(1,1) model, and the combined AR(2)+GARCH(1,1) model produced by our earlier analysis and used MF-DFA to analyze their multifractal properties. All three models appeared more monofractal than the original GE data that they are supposed to represent. The AR(4) model indicated a strong antipersistence, with the majority of Hölder exponents clustered around $\alpha = 0.25$, while the GARCH(1,1) model and the combined model both exhibited Hölder exponents clustered closer to where the GE data multifractal spectrum peaks at $\alpha = 0.51$ (see Figure 16). However, they both failed to achieve the range of Hölder exponents seen in the GE data.

6. Conclusion

During the twentieth century, economists relied heavily on Brownian motion to construct theoretical models of finance. The advantages of using Brownian motion stem from its foundation in the Gaussian distribution; and with advances in stochastic calculus and differential equations, it became a staple in models of empirical finance. The well-known Black-Scholes model for options pricing is a prime example of this application [6]. The Gaussian is a thin-tailed distribution such that a random variable sampled from it rarely exceeds six standard deviations from the mean. Even a cumulative sum of an extremely large number of such

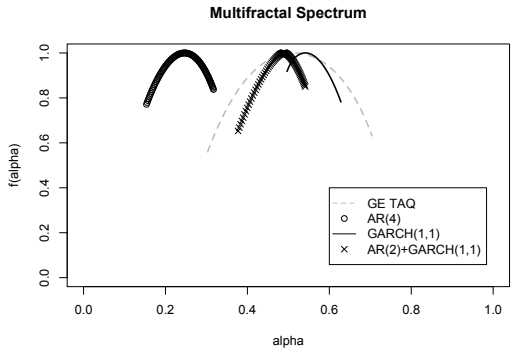

Fig. 16. The multifractal spectra of the GE TAQ data, the simulated AR(4) data, the simulated GARCH(1,1) data, and the combined AR(2)+GARCH(1,1) data.

variables fails to capture the erratic nature of some real processes like prices or log-prices of financial assets. Given that multifractal analysis has the ability to illuminate the underlying difference between a monofractal like Brownian motion and a considerably more diverse construction like the binomial measure, we contend it must find its place in financial theory. The obvious obstacle to this incorporation is the departure from the tractable closed-form mathematics associated with Gaussian measures. However, with advances in computing power, it is our belief that the impact of this obstacle can be minimized if not eliminated.

In the preceding analysis, we saw that traditional models applied to very fine-scale raw data tend to underestimate the multifractal properties of financial time series. What is interesting to note is the presence of both antipersistence and long memory in the GE TAQ data. This phenomenon underscores the concept of trading time. Small fluctuations might exhibit long memory, as they represent the normal fluctuations of a stock price on a slow news day. But large fluctuations exhibit antipersistence as groups of investors overreact and overcompensate to information they believe will have a more drastic impact on the asset's price. Although this is a convenient and plausible explanation for the properties we saw in the GE TAQ data, it begs the question of whether it can be supported by empirical analysis or not.

There is continuing debate over which parametric models best describe heavy-tailed returns and volatility clustering that are exceedingly common in financial time series. Mandelbrot suggested that we relinquish our reliance on the Gaussian approach started by Bachelier over a century ago, and focus on the scale invariant properties that are ubiquitous in finance [16]. His pioneering work in fractal geometry paved the way for this analysis, and with advances in computing power, we can extract multifractal properties from data in a matter of seconds. It is our contention that multifractal analysis should become a standard technique for analyzing complex systems, along side the other parametric approaches that often have difficulty capturing

the multiscaling nature of certain time series.

References

[1] L. Bao, J. Ma, W. Long, P. He, T. Zhang, A.V. Nguyen, Fractal analysis in particle dissolution: a review, Rev. Chem. Eng. 30 (2011) 261–287.

[2] J. Beran, Statistics for Long-Memory Processes, Chapman & Hall/CRC, Roca Raton, FL, 1994.

[3] T. Bollerslev, Generalized autoregressive conditional heteroskedasasticity, J. Econ. 31 (1986) 307–327.

[4] G.E.P. Box, G.M. Jenkins, G.C. Reinsel, Time Series Analysis: Forecasting and Control, fourth ed., John Wiley & Sons, Inc., Hoboken, NJ, 2008.

[5] L. Calvet, A. Fisher, Multifractality in asset returns: theory and evidence, Rev. Econ. Stat. 84 (2002) 381–406.

[6] A. Etheridge, A Course in Financial Calculus, Cambridge University Press, Cambridge, 2002.

[7] K. Falconer, Fractal Geometry: Mathematical Foundations and Applications, second ed., Wiley, Hoboken, NJ, 2003.

[8] E.F. Fama, Efficient capital markets: II, J. Finance, 46 (1991), 1575–1617.

[9] J. Feder, Fractals, Plenum Press, New York, 1988.

[10] M. Frame, B.B. Mandelbrot, N. Neger, Fractal geometry, Retrieved from http://classes.yale.edu/fractals, 2014.

[11] J.W. Kantelhardt, E. Koscielny-Bunde, H.H.A. Rego, S. Havlin, A. Bunde, Detecting long-range correlations with detrended fluctuation analysis, Phys. A 295 (2001) 441–454.

[12] J.W. Kantelhardt, S.A. Zschiegner, E. Koschielny-Bunde, S. Havlin, A. Bunde, H.E. Stanley, Multifractal detrended fluctuation analysis of nonstationary time series, Phys. A 316 (2002) 87–114.

[13] M.E. Kuhl, S.G. Sumant, J.R. Wilson, An automated multiresolution procedure for modeling complex arrival processes, INFORMS J. Comput. 18 (2006) 3–18.

[14] B. Lashermes, P. Abry, P. Chainais, New insights into the estimation of scaling exponents, Int. J. Wavelets Multiresolut. Inf. Proc. 2 (2004) 497–523.

[15] R. Lopes, P. Dubois, I. Bhouri, M.H. Bedoui, S. Maouche, N. Betrouni, Local fractal and multifractal features for volumic texture characterization, Pattern Recognit. 44 (2011) 1690–1697.

[16] B.B. Mandelbrot, The variation of certain speculative prices, J. Bus. 36 (1963) 394–419.

[17] B.B. Mandelbrot, The Fractal Geometry of Nature, W. H. Freeman and Company, New York, 1977.

[18] B.B. Mandelbrot, Multifractal measures, especially for the geophysicist, Pure Appl. Geophys. 131 (1989) 5–42.

[19] B.B. Mandelbrot, J.W. van Ness, Fractional Brownian motions, fractional noises and applications, SIAM Rev. 10 (1968) 422–437.

[20] R.F. Mulligan, R. Koppl, Monetary policy regimes in macroeconomic data: an application of fractal analysis, Q. Rev. Econ. Finance 51 (2011) 201–211.

[21] E. Onali, J. Goddard, Are European equity markets efficient? New evidence from fractal analysis, Int. Rev. Financ. Anal. 20 (2011) 59–67.

[22] C.-K. Peng, S.V. Buldyrev, S. Havlin, M. Simons, H.E. Stanley, A.L. Goldberger, Mosaic organization of DNA nucleotides, Phys. Rev. E 49 (1994) 1685–1689.

[23] M.S. Taqqu, V. Teverovsky, Estimators for long-range dependence: an empirical study, Fractals 3 (1995) 785–798.

[24] C. Thamrin, G. Stern, U. Frey, Fractals for physicians, Paediatr. Respir. Rev. 11 (2010) 123–131.

[25] J.R. Thompson, J.R. Wilson, Multifractal analysis of agent-based financial markets, in: R. Pasupathy, S.-H. Kim, A. Tolk, R. Hill, M.E. Kuhl (Eds), Proceedings of the 2013 Winter Simulation Conference, Institute of Electrical and Electronics Engineers, Piscataway, NJ, 2013, pp. 1383–1394.

[26] J.R. Thompson, J.R. Wilson, Agent-based simulations of financial markets: zero- and positive-intelligence models, Technical report submitted for publication. Edward P. Fitts Department of Industrial and Systems Engineering, NC State University, Raleigh, NC, 2014. Retrieved from www.ise.ncsu.edu/jwilson/files/absfm14.pdf.

[27] J.R. Thompson, J.R. Wilson, Online appendix to "Multifractal detrended fluctuation analysis: practical applications to financial time series." Technical report submitted for publication, Edward P. Fitts Department of Industrial and Systems Engineering, NC State University, Raleigh, NC, 2014. Retrieved from www.ise.ncsu.edu/jwilson/files/mfdfa-oa.pdf.

[28] B.F. Tivnan, M.T.K. Koehler, M. McMahon, M. Olson, N.J. Rothleder, R.R. Shenoy, Adding to the regulator's toolbox: Integration and extension of two leading market models; in: G. Loury (Ed), Proceedings of the 2011 Annual Conference of the Eastern Economic Association, Ramapo College, Mahwah, NJ, 2011, pp. 1–13.

[29] Wharton Research Data Services, retrieved from http://wrds-web.wharton.upenn.edu/wrds/, 2013.

[30] D. Wuertz, Y. Chalabi, Rmetrics - autoregressive conditional heteroskedastic modelling, in: R: A Language and Environment for Statistical Computing, Version 3010.82: Revision 5504, retrieved from http://www.rmetrics.org, 2013.

[31] D. Wuertz, Y. Chalabi, ARMA time series modelling, in: R: A Language and Environment for Statistical Computing, Version 3010.79: Revision 5527, retrieved from http://www.r-project.org, 2013.